Influences of root-induced soil suction and root geometry on slope stability: a centrifuge study

Leung, Anthony; Kamchoom, V.; Ng, C. W. W.

Published in:
Canadian Geotechnical Journal

DOI:
10.1139/cgj-2015-0263

Publication date:
2016

Document Version
Peer reviewed version

Influences of root-induced soil suction and root geometry on slope stability: a centrifuge study

Leung, Anthony; Kamchoom, V.; Ng, C. W. W.

Published in:
Canadian Geotechnical Journal

DOI:
10.1139/cgj-2015-0263

Publication date:
2016

Document Version
Peer reviewed version

Influences of root-induced soil suction and root geometry on slope stability: a centrifuge study

A. K. Leung, V. Kamchoom* and C. W. W. Ng

Name: Dr Anthony Kwan, LEUNG

Title: Lecturer

Affiliation: Division of Civil Engineering, University of Dundee

Address: Division of Civil Engineering, University of Dundee, Nethergate, Dundee, UK

Name: Dr Viroon, KAMCHOOM* (Corresponding author)

Title: Post-Doctoral fellow

Affiliation: Department of Civil and Environmental Engineering, Hong Kong University of Science and Technology

Address: Department of Civil and Environmental Engineering, Hong Kong University of Science and Technology, Clear Water Bay, Kowloon, Hong Kong

Email: kviroon@ust.hk

Name: Dr Charles Wang Wai, NG

Title: Chair Professor of Civil Engineering

Affiliation: Department of Civil and Environmental Engineering, Hong Kong University of Science and Technology

Address: Department of Civil and Environmental Engineering, Hong Kong University of Science and Technology, Clear Water Bay, Kowloon, Hong Kong

Abstract:

Soil bioengineering using vegetation has been recognised as an environmentally friendly solution for shallow slope stabilisation. Plant transpiration induces suction in the soil, but its effects to slope stability are often ignored. This study investigates the influences of transpiration-induced suction and mechanical reinforcement of different root geometries (i.e., tap- and heart-shaped) to the slope stability subjected to an intense rainfall with an intensity of 70 mm/h (prototype scale; corresponding to a return period of 1000 years), via centrifuge modelling. New model roots that have scaled mechanical properties close to real roots were used to simulate transpiration-induced suction in the centrifuge. Transient seepage analyses were performed using SEEP/W to back-analyse the suction responses due to transpiration and rainfall. Subsequently, the back-analysed suction was used to assess the factor of safety of the slopes using SLOPE/W. It is revealed that heart-shaped roots provided greater stabilisation effects to a 60^{o} clayey sand slope than tap-shaped roots. The heart-shaped roots induced higher suction, leading to 14% reduction of rainfall infiltration and 6% increase in shear strength. Although transpiration-induced suction in a 45^{o} slope was reduced to zero after the rainfall, mechanical root reinforcement was found to be sufficient to maintain the slope stability.

Keywords:

Slope stability; Plant transpiration; Suction; Root geometry; Unsaturated soils; Centrifuge modelling

Introduction

Vegetation has been generally recognised as an environmentally friendly alternative that could be used for ecological restoration (Hau and Corlett 2003) and also enhance slope stability against rainfall (Barker 1995; Greenwood et al. 2004). Plant roots exist in soil as inclusion to increase the mechanical strength of shallow soil, as have been demonstrated by various direct shear tests (Docker and Hubble 2008; Ghestam et al. 2013) and pull-out tests (Mickovski and Ennos 2003; Burylo et al. 2009). Centrifuge modelling technique has also been adopted to test to what extent plant roots could mechanically reinforce soil slope (Sonnenberg et al. 2010). This technique enables scaled physical model slopes to be tested at the stress levels close to those experienced by much larger prototypes. In order to have better controlled test conditions, some idealised, yet representative, model roots (Stokes and Mattheck 1996; Sonnenberg et al. 2012) have been developed and used to study the fundamental mechanical soil-root interaction. Sonnenberg et al. (2012) applied their model roots in centrifuge tests to quantify the mechanical slope reinforcement.

Although there is a large body of research focusing on the mechanical effects of roots on slope stability like steel reinforcements, any hydrological effects of root transpiration resulting in a change of soil suction on soil shear strength and reduction in hydraulic conductivity have been generally overlooked. It is well-known that plant would transpire and the associated root-water uptake would increase soil suction (Barker 1995; Greenwood et al. 2004; Leung and Ng 2013). It has been identified from various field and laboratory tests that a higher suction could be preserved in vegetated soil than that in bare soil (Lim et al. 1996; Simon and Collison 2002; Ng et al. 2013, 2014a; Leung and Ng 2015; Leung et al. 2015; Garg et al. 2015, among others). An increase in suction would lead to the increase in soil shear strength and also the decrease in soil hydraulic conductivity (Ng and Leung 2012). Numerical and analytical studies (Yuan and Lu 2005; Zhu and Zhang 2014; Ng et al. 2015) showed that the magnitude and distribution of transpiration-induced suction could be affected by root geometry substantially, but this has yet to be verified by physical tests. Recently, Kamchoom et al. (2014) and Ng et al. (2014b) designed some new model roots with different geometries. These new model roots are capable of simulating the effects of transpiration and creating credible suctions typically found in the field. Kamchoom et al. (2014) showed that for a given root geometry, the pull-out resistance of roots would increase significantly when transpiration-induced suction was taken into account. More

recently, Ng et al. (2015) adopted the new root models developed by Ng et al. (2014b) to study the effects of three different root geometries, namely tap-, heart- and plate-shaped, on the stability of 45^o slopes in a centrifuge. They concluded that the tap- and heart-shaped root geometries provided the greatest stability of the slopes. Although these two root geometries were able to stabilise 45^o slopes, their effectiveness to reinforce ever more steep slopes that are commonly found in crowded urban cities like Hong Kong is not known.

This study aims to evaluate whether the tap- or heart-shaped root geometries could stabilise 60^o slopes or not. If not, what failure mechanisms can be revealed and identified. Any differences in the distributions of transpiration-induced suction and failure mechanisms between 45^o and 60^o slopes are compared and investigated. Observed slope hydrology under the effects of "transpiration" and rainfall was interpreted through finite element transient seepage analyses, the results of which were then subsequently used for assessing factor of safety (FOS; at ultimate limit state) of each model rooted slope.

Centrifuge modelling and testing

Test plan

Three centrifuge tests were conducted at 15$\boldsymbol{g}$ in the geotechnical centrifuge facility at the Hong Kong University of Science and Technology. By using centrifuge, testing a 1:N model at N times of the Earth's gravity through centripetal acceleration would recreate stress levels that are close to much larger full-scale prototype systems (Taylor 1995). In this way, the mechanical soil behaviour, which chiefly depends on confining pressure, in the 1:N model would hence be correctly captured.

The first two centrifuge tests aim to evaluate the effectiveness of using tap-shaped root geometry to stabilise soil slopes with two different gradients, 45^o and 60^o (denoted as Tests T45 and T60, respectively). As the model slope in Test T45 remained standstill after testing (discussed later), it was decided to further test a steeper slope angle of 60^o in Test T60. Previous experiment conducted by Zhou (2008) has shown that a bare slope comprising the same soil type could not maintain its stability when roots are absent. Such steep slope condition also represents an extreme condition, where plants could perceive considerable root growth for shallow stabilisation (Miles and Sheila 1986; Chiatante et al. 2003). The third test investigated a 60^o slope supported by heart-shaped root geometry (denoted as Test H60). Thus, comparisons of the

results obtained from Tests T60 and H60 could evaluate which root geometry provides greater stabilisation effects to the 60^o slope.

Test material

The soil used for testing is completely decomposed granite (CDG; categorised as clayey sand (CL) according to ASTM D2487-11 (2011)), which is commonly found in Hong Kong. In order to minimise any particle-size effects in centrifuge tests (Taylor 1995), CDG with particle sizes larger than 2 mm were sieved. This resulted in 56.8% sand content and 43.2% fines. The D_{50} of the soil was 0.081 mm. For the given diameter of model root (i.e., D_r of 6 mm in model scale), the ratio D_r/D_{50} was 74. This ratio was well above 30, which was identified to be the upper limit that the particle size effects might become insignificant (Bolton et al. 1993). The plastic limit and liquid limit of the soil is 22.7% and 32.8%, respectively. The effective cohesion (c') and effective critical-state friction angle (ϕ') of the CDG is zero and 37.4^o, respectively. Falling-head tests showed that the saturated hydraulic conductivity (k_s) of CDG compacted at a dry density of 1777 kg/m^3 or relative compaction (RC) of 95% (i.e., the targeted value in this study) was 1 x 10^{-7} m/s. A pair of drying and wetting soil water retention curves (SWRCs) of the CDG was measured using a pressure-plate apparatus. As shown in Fig. 1, the air-entry value (AEV) of the CDG was 1 to 2 kPa, beyond which the volumetric water content (VWC) reduced substantially. The SWRC is found to be hysteretic as the VWC along the wetting curve is always lower than that along the drying one. Some measured index properties of CDG are summarised in Table 1.

Model roots used for centrifuge testing

The new model roots designed by Kamchoom et al. (2014) and Ng et al. (2014b) were used in each centrifuge test. The overview of the model roots is depicted in Figs 2(a) and (b), with all dimensions expressed in prototype scale. Two root geometries were studied, namely tap- and heart-shaped, according to the idealisation and categorisation of plant root systems made by Stokes and Mattheck (1996). Tap- and heart-shaped roots are considered to be representative to the field observation of real roots of *Schefflera heptaphylla* and *Rhodomyrtus tomentosa*, respectively. They are two common species that has been identified for slope bioengineering and ecological restoration in tropical and subtropical regions (Hau and Corlett 2003; Leung 2014). Fig. 3 compares the distribution of Root Area Ratio (RAR; defined as the cross-sectional area ratio between roots and soil along depth) between artificial and some real roots. It can be seen

that RARs of real roots are reasonably replicated by artificial model roots, given the natural variability of plants in the field. As shown in the figure, it is not uncommon to identity a typical root depth of 0.75 m in the field. For examples, in subtropical and tropical regions, root depths are generally shallow since ample rainwater is available near the ground surface for transpiration (Ray and Nicoll 1998; Huang 1999). Also, for steep slopes (like 60^o in this study), various studies have shown that the maximum depth that vegetation could perceive is 0.75 m (Miles and Sheila 1986; Chiatante et al. 2003)

Cellulose acetate (CA) was chosen to construct each model root. CA has an elastic modulus (E) of 83 MPa and a tensile strength (σ_t) of 31 MPa, both of which are fairly close to those typically identified in real roots (Stokes and Mattheck 1996). In this study, the axial rigidity (EA, where A is the cross-section area) of each model root was scaled, instead of flexural rigidity (EI, where I is the second moment of inertia). This is because the primary mechanism of root reinforcement against slope failure was associated with axial strain mobilisation, whereas any bending strain was little (Sonnenberg et al. 2012). For the scaling factor of $1/N^2$ (Taylor 1995), the prototype EA at $15\boldsymbol{g}$ is 0.290 MPa-m^2. Figure 4 compares the prototype EA of CA with some real tree roots and other materials that have been previously selected for constructing model roots for geotechnical investigation. It can be seen that the EA of CA lies within the bounds and represents the average value of the database.

A series of direct shear tests were conducted to determine the soil-model root interface properties. The results showed that both the peak and ultimate interface friction angle are 34^o (Kamchoom et al. 2014), which is close to the typical range (36.1^o – 37.9^o) for a soil-real root interface (Wang et al., 2010). Centrifuge pull-out tests using the design of model roots were also conducted and found that the peak pull-out resistance and post-peak behaviour of both tap- and heart-shaped roots were consistent with the field observation (Kamchoom et al. 2014). Table 2 summarises all the relevant scaling laws and root properties.

In order to simulate the effects of transpiration-induced suction in centrifuge, each model root was connected to the suction-controlled system developed by Ng et al. (2014b) (Fig. 2(c)). Each model root consists of a porous filter (CA in this study), which is connected to an air-tight chamber where vacuum pressure is supplied by an aspirator system. The filter has a high AEV and is water-saturated for (i) maintaining hydraulic connection between the system and the surrounding soil and (ii) preventing air from entering the system (as long as the applied vacuum

pressure is lower than the AEV of the filter). Any decrease in soil moisture due to the applied vacuum hence induces suction. Besides being a suitable material for modelling the mechanical properties of real roots, CA is also an appropriate porous filter material for simulating the effects of transpiration. This is because CA has an AEV of 100 kPa, which is higher than the maximum vacuum pressure produced by the system (i.e., 95 kPa). It should be noted that it is not the intention of the design of the system to mimic the actual physiological plant-water relation in centrifuge. The system has been demonstrated to be capable of recreating the magnitude and distribution of suction reasonably close to some field measurements (Ng et al. 2014b).

Model package and preparation

Figure 5 shows the centrifuge model setup for Tests T45 and T60. All model slopes have an identical height of 6.4 m. Before compacting each model slope, the centrifuge strong box was laid down on the floor. A thin layer of silicon grease is pasted on the internal walls of the strong box as well as the perspex to minimise any interface friction (Powrie 1986). A wooden mould that has a shape identical to the slope geometry was fitted inside the strong box, and the sieved CDG was compacted by moist tamping at the RC of 95%. Undercompaction method (Ladd 1977) was used to compact the soil with gravimetric water content of 15.1% in six layers. When the soil was compacted to the first, third and fifth layers, an array of five model roots were placed on the soil surface and oriented perpendicular to the slope face. The root spacing was set to be 1.73 m (in prototype). This is to ensure that the Root Area Ratio (i.e., RAR, the ratio of cross-sectional area of roots to that of the soil at a given depth) is consistent with the field observation (Kamchoom et al. 2014). The subsequent soil layer was compacted to ensure each model root having proper contact with the surrounding soil. Following these procedures resulted in a total of 15 roots that were arranged in a square pattern (3 columns x 5 rows). Each model root was then connected to the suction-controlled system via a vacuum delivery panel (Fig. 2(c)).

Regarding the hydraulic boundary conditions, the bottom and side boundaries of each strong box were set to be impermeable. The slope surface and the crest surface were left exposed for rainfall infiltration. In order to produce and control a rainfall event during a test, a rainfall simulation system was developed. It consisted of six nozzles that were mounted to the lid of the strong box. All nozzles were connected to a built-in chamber that could store a maximum amount of 50 l of water. During each simulation of rainfall, the water stored in the chamber would be pressurized and sprayed through the nozzles in the form of mist. The use of mist to simulate

rainfall aims to minimize the impact energy on the soil surface (Caicedo and Tristancho 2010). Prior to testing, the rainfall simulation system was calibrated to minimise the Coriolis effect at 15g (i.e., the g-level adopted in this study). In order to produce a uniform rainfall with an intensity of 70 mm/h (i.e., the intensity applied in this study), the nozzles were designed to orientate vertically and arranged in 2 rows x 3 columns. For Tests T45, T60 and H60, the nozzle spacing was set to be 158, 147 and 147 mm, respectively. All six nozzles in three tests were fixed at 83 to 85 mm above the soil surface. By using this nozzle arrangement, a pressure of 450 kPa was needed to apply to the water chamber so as to produce a rainfall with an intensity of 70 mm/hr. This resulted in a spray angle of approximately 165^{o}. For the given water volume in the chamber (i.e., 50 l), the minimum and maximum rainfall intensity that can be created by the system is 40 mm/hr (for 88 hours) and 93 mm/hr (for 37 hours) in prototype scale, respectively. After attaching the system, a wind cover was placed over the strong box to minimise any evaporation from the bare soil surface.

Instrumentation

In each model slope, an array of three pore-pressure transducers (PPTs; Druck PDCR-81), namely P1 to P3, were used to monitor the responses of PWP during testing (Fig. 5). The porous stone attached to each PPT was replaced with an 1-bar AEV ceramic filter. Prior to installation, a cylindrical rod with a diameter slightly smaller than that of a PPT was used to drill horizontally from the back of strong box into the location of each PPT. At the mid-section of each model slope, the three PPTs were installed at depths of 0.3 m, 0.6 m and 1.2 m perpendicular to the slope surface 0.45 m from the model root.

During an applied rainfall event, any surface runoff generated from each model slope was collected and measured using a runoff collection frame attached near the slope toe. A PPT (P4) was mounted inside the frame for monitoring any build-up of water pressure due to the accumulation of runoff water. As a result, the infiltration rate in the model slopes can be determined by the difference between applied rainfall intensity and measured runoff. In addition, failure mechanism of each model slope along the plane of symmetry (i.e., on the Perspex wall) was captured by high-speed and high-resolution cameras.

Test procedures

Each centrifuge test consisted of five stages. The first stage was to spin the centrifuge model

package (waypoint A), until the centrifugal acceleration reached 15***g*** (waypoint B). In the second stage, the 15***g*** acceleration was maintained until any change in PWP was less than 1 kPa (i.e., accuracy of each PPT) within 24 hours in prototype (waypoint C). This aimed to allow the soil mass to consolidate and to dissipate any excess PWP that might have generated during the previous rising ***g*** level. When an equilibrium was reached at 15***g***, no more seepage due to the centrifuging took place in the slope. Any observed changes in PWP in the subsequent stages were attributed to the effects of water uptake by model roots and rainfall. The third stage was to simulate the effects of transpiration using the suction-controlled system by applying a vacuum pressure of 95 kPa to all model roots. The use of this particular vacuum pressure has proven to be able to create a range of suction that was observed in the field reasonably well (Ng et al. 2014b). The vacuum pressure was then kept constant, until all PPTs showed less than 1 kPa change in PWP within 24 hours in prototype (waypoint D). In the fourth stage, a rainfall event was simulated. A constant rainfall intensity of 70 mm/h with a duration of 8 h (in prototype; waypoint E) was applied in all tests. The selected rainfall intensity refers to the threshold for issuing a black rainstorm signal by the Hong Kong Observatory (Li and Lai 2004). The risk level of this signal is the highest and rainfall under this condition is prone to inducing landslides in Hong Kong (GEO 2002). The rainfall pattern gave a return period of 1000 years, according to a statistical analysis conducted for Hong Kong's rainfall data (Lam and Leung 1995). The last stage (waypoint F) was to spin down the model package back to 1***g***. Some details of the two centrifuge tests are listed in Table 3.

Numerical modelling

Analysis plan and modelling approaches

Three series of seepage-stability analyses were carried out to interpret the three centrifuge tests. Each analysis first back-analysed measured responses of PWP induced by the model roots using SEEP/W (Geo-Slope Int., 2009), and then the back-analysed results were utilised to calculate the factor of safety (FOS) using SLOPE/W (Geo-Slope Int., 2008). SEEP/W is a finite element software that can simulate transient seepage in non-deformable soil through Richards equation, while SLOPE/W uses limit equilibrium method to determine FOS for some pre-defined slip surfaces based on the PWP computed from SEEP/W.

Typical finite element meshes for modelling Tests T45 and H60 are shown in Fig. 6, both

analysed in prototype scale. For the purpose of back-analyses, the slope geometry and root arrangement in all numerical models were set to be identical to the centrifuge test setup. All the boundaries of each model slope were specified to be impermeable, except the slope crest and slope face, where the measured infiltration rate (as given later) was applied.

In order to simulate the three-dimensional (3D) water uptake process by the model roots, equivalent two-dimensional (2D) plane-strain analyses were conducted using SEEP/W. First of all, at each location of model root, the CA filter was modelled by creating a material that has an AEV of 100 kPa and a saturated hydraulic conductivity of 2×10^{-6} m/s (see inset). Then, the dimension of the internal spacing of the CA was adjusted so that the total capacity of water volume flow in this 2D plane-strain "root wall" is equal to that in the 3D circular root tested in the centrifuge, following the approach suggested by Indraratna and Redana (1997). The adjusted dimension of the CA is shown in Fig. 6(a). Finally, a constant pressure head was applied along the internal boundary of the CA to simulate the effects of transpiration. Although a constant vacuum pressure of 95 kPa (i.e., -9.5 m pressure head) was applied in all the experiments, the elevation head difference between the model roots and the water level in the vacuum chamber (Fig. 2(c)) must be corrected in the numerical modelling. The corrected constant pressure head applied in each model root is shown in Fig. 6. In each model root, the pressure head was applied along the internal wall of the CA (see inset).

For the modelling of the mechanical properties of each component (i.e., tap and branch) of a model root in SLOPE/W, the CA filter was replaced by soil material. A representative cable element of each model root was used to capture the elastic axial response. It should be noted that neglecting any flexural strength provided by model roots is deem acceptable because it has been experimentally identified that any mobilisation of bending moment of roots was little against pull-out (Kamchoom et al. 2014) and slope movement (Sonnenberg et al. 2012). When modelling each heart-shaped root, the connection between the taproot component and the two branches was rigid. It was assumed that the interface friction between soil and each model root was fully mobilised and evenly distributed along all root components, as have been observed by Sonnenberg et al. (2012). This modelling method is capable to simulate structural elements (such as nails/roots) that are rigid relative to the stiffness of the surrounding soil (Geo-Slope Int., 2008). The reinforcement load in each cable element was computed by multiplying the surface area of each root component by the interface frictional strength determined by the direct shear tests (i.e.,

interface friction angle of 34^o). In all the SLOPE/W analyses, the reinforcement load is considered as contributing to reducing the destabilising force, and the FOS is calculated accordingly.

Input soil parameters

Soil water retention curve (SWRC) and hydraulic conductivity function (HCF) are required for conducting a seepage analysis. The measured drying and wetting SWRCs (Fig. 1) were fitted with the equation proposed by van Genuchten (1980). The drying and wetting HCFs were then estimated using the prediction equation proposed by van Genuchten (1980), based on the fitting coefficients obtained from SWRCs and the measured k_s (1 x 10^{-7} m/s).

For each slope stability analysis, CDG was modelled as a perfectly-plastic material that obeys the Mohr-Coulomb failure criterion suggested by Vanapalli et al. (1996), as follows:

$$\tau_s = c' + (\sigma_n - u_a)tan\emptyset' + (u_a - u_w)\left[\left(\frac{\theta_w - \theta_r}{\theta_s - \theta_r}\right)tan\emptyset'\right] \quad (1)$$

where τ_s is soil shear strength; σ_n is normal stress on a slip surface; u_a is pore-air pressure (taken to be atmospheric); u_w is PWP; θ_w is VWC; θ_s is VWC at saturation; and θ_r is VWC at residual state. Note that θ_w in Eq (1) was determined by mapping the suction computed by SEEP/W to the SWRC inputted. The two shear strength parameters of the CDG, *c'* and ϕ', are respectively taken to be zero and 37.4^o based on the laboratory measurements.

Analysis procedures

The numerical simulations of transient seepage followed the identical procedures of the three centrifuge tests. Each seepage analysis consisted of three stages. The first stage was to create an initial suction distribution in each numerical model that was similar to that observed in each centrifuge test right before the simulation of transpiration (i.e., at waypoint C). This was achieved through a trial-and-error process by adjusting the depth of a water table so that the hydrostatic distribution of PWP was close to the centrifuge measurements made at all PPT locations. Extensive numerical effort showed that setting a water table (see Fig. 6) at the depths of 3.0 m, 4.5 m and 4.5 m gave the closest steady-state suction to those found in Tests T45, T60, H60, respectively. The second stage was to simulate the "transpiration" happened in each test (waypoints C to D) by applying a constant pressure head in the CA filter. In this stage, the drying SWRC and HCF were used. Then, the third stage of analysis was to apply the measured

infiltration rate at the slope crest and the slope face for simulating the applied rainfall event. In order to capture the effects of hysteresis on PWP responses, the wetting SWRC and HCF were inputted in this stage.

After performing each transient seepage analysis using SEEP/W, the back-analysed PWP responses were inputted to SLOPE/W for stability calculation. For slopes that did not show any failure in centrifuge, minimum FOS (FOS_{min}) for a critical slip surface was determined. On the contrary, when slope failure was observed in any test, the identified slip surface was manually specified to determine the FOS. In all stability calculations, Janbu's method was adopted because this method satisfies both the horizontal and vertical force equilibria. This is essential to resolve both the horizontal and vertical components of axial force mobilised by each model root for resisting a pre-defined slip surface.

Interpretation of measured and computed results

Responses of pore-water pressure during the simulation of transpiration

The measured variations of PWP with time for the Tests T45, T60 and H60 are depicted in Figs 7(a), (b) and (c), respectively. Before subjecting to centrifuging, the initial suction (or negative PWP) recorded by all PPTs was 15 kPa in all three tests. During the process of rising $\boldsymbol{g}$ level and the consolidation, the PWP responses were largely similar between the three tests. The increases in PWP during the centrifuging (waypoints A-B) were attributed to the building up of excess PWP, which was then dissipated during the subsequent self-weight consolidation (waypoints B-C). It can be seen from Figs 7(d), (e) and (f) that after consolidation, the PWP distributions from all three tests followed the hydrostatic line quite closely. This suggests that a water table exist in each slope. The computed PWP profiles (dashed lines) are also shown in Figs 7(d), (e) and (f) for direct comparison with the centrifuge measurements. It can be seen that by specifying a water table in the numerical model slopes, the PWP distribution before transpiration matched well with the measurements. At the end of 15$\boldsymbol{g}$ consolidation, all slopes remained standstill in the centrifuge. The centrifuge observation agreed with the stability calculation that the computed FOS_{min} for all three cases was higher than 1.0.

When the effect of transpiration was simulated (waypoints C-D) in the centrifuge, the measured suction within the root zone (i.e., top 0.6 m) increased in all three model slopes, whereas that below root zone (i.e., 1.2 m) remained almost unchanged. This is more clearly seen

when presenting the PWP data along depths (Figs 7(d), (e) and (f)). In both Tests T45 and T60, the decreases in PWP at 0.3 m and 0.6 m depths were similar to each other (Figs 7(d) and (e)). However, in Test H60 (Fig. 7 (f)), the decrease in PWP at 0.3 m depth was more than that at 0.6 m depth. The computed PWP profiles (dashed lines) also matched the measurements made in all three tests. In the numerical simulations, the heart-shaped roots also produced higher suction than the tap-shaped roots. When compared to tap-shaped root, each heart-shaped root has two additional root branches (Fig. 2), which therefore provided greater hydraulic contact with the surrounding soil to induce a higher suction. This highlights the significance of the role of root geometry in affecting both the magnitude and the distribution of induced suction. Because of the "transpiration"-induced suction, the computed FOS_{min} of the two 60^o slopes increased from 1.2 to 1.3 fairly slightly (Figs 7(a) and (b)), whereas that of the 45^o slope maintained at about 1.8 (Fig. 7(c)). In fact, the critical slip surface identified in Test T45 after "transpiration" (given later) was at depths much greater than the root zone. Thus, the suction increase near the root zone did not result in significant change in FOS_{min}.

Infiltration characteristics and suction responses of vegetated soil during rainfall

The measured variations in the water infiltration rate with time among the three slopes are compared in Fig. 8. The infiltration rates observed in all three slopes exhibited exponential reduction, gradually approaching the k_s of the CDG (i.e. 1×10^{-7} m/s). As expected, the two 60^o slopes have lower infiltration rate than the 45^o slope. When comparing the responses obtained from Tests T60 and H60, the latter case showed lower infiltration rate, despite of the same slope angle. This is because the suction induced before the rainfall event in Test H60 was higher (Figs 7(e) and (f)), which would hence lead to greater reduction of soil hydraulic conductivity (Fig. 1). For conducting seepage analysis, each infiltration rate was best-fitted and then imposed on the slope face boundary in SEEP/W for simulating the wetting event.

Figures 9(a), (b) and (c) depict the measured PWP responses upon rainfall infiltration in the three centrifuge tests. In general, the PWPs within the root zone (i.e., top 0.6 m depth) in all three slopes showed significant increases during the first 1.5 h of rainfall, whereas the PWP at the greater depth of 1.2 m increased rather gradually. In Test T60, shallow slope failure happened after 3 h of rainfall when the PPT at 0.3 m depth recorded 3 kPa of suction (Fig. 9(b)). The PPT then lost contact with the surrounding soil. Further shallow slope failure happened near 5 h of rainfall when the suction at 0.6 m depth reached 6 kPa. This PPT also lost contact subsequently.

In Test H60, shallow slope failure also took place, but at the relatively later stage after 5 h of rainfall (Fig. 9(c)). After subjecting to the intense rainfall for 8 h, no suction was left in all tests, but all three slopes remained standstill without showing any global or deep-seated type of failure.

By comparing the PWP profiles between Tests T45 and T60 (Figs 9(d) and (e)), the measured PWPs after 3 h and 5 h of rainfall in the latter case were always higher, by not more than 3 kPa though. This is mainly because there was relatively less volume of water infiltrated into the steeper slope in Test T60 (Fig. 8). When the 60^o slope was supported by heart-shaped roots (Fig. 9(f)), the measured suction retained at all three depths was markedly higher than the other two cases after 5 h of rainfall. This was attributed to the higher suction induced by this particular root geometry during the previous drying period, which had resulted in lower infiltration rate (Fig. 8). The computed PWP profiles before and after rainfall were also depicted in Figs 9(d), (e) and (f) for comparison. It can be seen that the simulations matched the centrifuge measurements and they were able to capture the measured reduction of PWP. This suggests that the modelling approach adopted in this study could simulate the effects of hysteresis reasonably well, and hence back-analyse the PWP responses during the wetting event fairly accurately. This provides confidence in utilising the back-analysed PWP responses to carry out the subsequent stability analyses reliably.

Discussion on slope failure mechanisms

Figures 10(a) to (c) show the images of slope responses in Test T45 before rainfall and after 3 h, 5 h and 8 h of rainfall, together with the critical slip surfaces computed from the stability analyses. Before rainfall (Fig. 10(a)), the slope was stable in the centrifuge. In the SLOPE/W analysis, the slip surface corresponding to the FOS_{min} of 1.81 formed at depths below the root zone. This means that the initial stability of the model slope was maintained, contributed by the shear strength of the soil (i.e., through ϕ') and the "transpiration"-induced suction (Eq. 1). After subjecting to the intense rainfall for 8 h, the slope remained stable in the centrifuge. The computed FOS_{min} dropped from 1.81 to 1.04 (Figs 10(b) to (c)), following the increases in PWP (Figs 9(a) and (d)). At the end of the rainfall event, the FOS_{min} was still higher than 1.0. As suctions induced by transpiration were disappeared (i.e., zero) after the rainfall (Figs 9(a) and (d)), the shallow stability of this particular slope was thus mainly contributed by the mechanical root reinforcement as well as the shear strength of the soil through ϕ'.

When the tap-shaped root geometry was used to support the 60^o slope (i.e., Test T60), the shallow stability was maintained only during the first 3 h of rainfall in the centrifuge (Fig. 10(d)). Shallow slope failure then happened near the slope crest (Figs 10(e) and (f)). In the stability analyses, the computed values of FOS after 3 h and 5 h of rainfall were both higher than 1.0, contradicting to the centrifuge observation. In fact, the slips observed in the centrifuge test were rather shallow, located at only 20 – 50 mm depth in model scale. This could be associated with surface erosion, rather than rotational slip presumed in the stability analyses. The Universal Soil Loss Equation (USLE; Wischmeier and Smith 1978) may be used to assess the potential of soil erosion. Since the rainfall event and soil type were identical in all three centrifuge tests, the only factor that controls the vulnerability of erosion is the slope angle. Design charts of USLE suggest that erosion is more susceptible for steeper slopes. This explains why erosion took place mainly in 60^o slope but not 45^o slope. More attention should be paid to select plants with appropriate vegetation cover if the slope is more susceptible to erosion. According to the cover-management factor in the USLE, vegetation coverage of more than 60% on a soil surface could reduce the amount of soil erosion substantially by 100 times (Wischmeier and Smith 1978).

When heart-shaped root geometry was used to support the 60^o slope (i.e., Test H60; Figs 10(g) to (i)), the centrifuge results show that the stability was maintained for a longer period of time than the case using tap-roots. No slope failure occurred in Test H60 during the first 3 h of rainfall, as consistently found in the slope stability analyses ($FOS_{min} > 1.0$). The greater stability provided by the heart-shaped root geometry was twofold. As revealed in Figs 9(c) and (f), the magnitude of suction retained in Test H60 during rainfall was always higher than that found in Test T60, resulting in higher mechanical soil strength (Eq 1). Moreover, the two branches of the heart-shaped root provided higher and more ductile pull-out resistance than the tap-shaped one, as have been shown by the centrifuge test results reported by Kamchoom et al. (2014). After 5 h of rainfall, a shallow slip that cut some model roots was observed at 20 – 50 mm depth in model scale in the centrifuge (Fig. 10(i)), as similarly found in T60 (Fig. 10(f)). The stability analysis for this specific slip showed that the computed FOS was higher than 1.0, again not consistent with the centrifuge observation. This indicated that the shallow slip observed in the 60^o slope in the centrifuge was likely to be the consequence of erosion.

A practical implication of this study is that tap-shaped roots could resist sliding-type of shallow failure of 45^o slopes, but this type of roots are ineffective for stabilising 60^o slopes which

failed mainly by erosion. Although erosion failure was also observed in the 60^o slope reinforced by heart-shaped roots, the slope stability could be maintained for a longer period of rainfall duration resulting from a higher transpiration-induced suction and mechanical resistance, as compared with slopes reinforced by tap-shaped roots.

Summary and conclusions

This paper investigated the effectiveness of using plant roots for shallow slope stabilisation, with dual consideration of transpiration-induced suction and mechanical root reinforcement. New model roots that have scaled mechanical properties reasonably close to real roots were used to simulate the effects of transpiration and to create suction in the centrifuge. Centrifuge model tests combined with seepage-stability analyses showed that tap-shaped root geometry was able to stabilise a 45^o slope for an intense rainfall event with a return period of 1000 years. Although no suction was preserved at the end of the rainfall, mechanical root reinforcement was revealed to provide sufficient stability to the shallow slope (i.e., within root zone), resulting in the values of FOS_{min} always larger than 1.0.

The tap-shaped root geometry was, however, less effective for stabilising the 60^o slope under the identical rainfall event. Shallow slope failure (i.e., slip found at 0.3 to 0.75 m depth in prototype scale) happened after 3 h of the intense rainfall event. When heart-shaped root geometry was used, the stability of the 60^o slope could be maintained for an increased period of rainfall duration for 5 h, beyond which some shallow slips also took place at similar depths. The delayed slope failure is mainly because the heart-shaped root geometry induced a higher suction than the tap-shaped root by at least 3 kPa. In addition to the taproot component, the heart-shaped root has two horizontal branches that provided additional hydraulic contact with the surrounding soil for more water uptake to take place. This thus led to at least 14% reduction of rainfall infiltration and about 6% increase in soil shear strength. Moreover, the horizontal branches also provided more ductile mechanical reinforcement due to the higher pull-out resistance and greater soil-root interface friction. The greater hydrological and mechanical effects provided by the heart-shaped roots hence resulted in greater shallow stability of the slope.

Acknowledgements

A research grant (HKUST6/CRF/12R) provided by the Research Grants Council of the Government of the Hong Kong SAR and another one (2012CB719805) provided by the Ministry

of Science and Technology of the People's Republic of China under the National Basic Research Program (973 Program) are acknowledged. The first author would also like to acknowledge the EU Marie Curie Fellowship provided under the Career Integration Grant for the project “BioEPIC”, and research travel support from the Northern Research Partnership. The second author also acknowledge the “Hong Kong-Scotland Partners in Post-Doctoral Research” (S-HKUST601/15) provided by the Research Grants Council of Hong Kong SAR and the Scottish Government.

References

Adhikari, A. R., Gautam, M. R., Yu, Z., Imada, S. and Acharya, K. 2013. Estimation of root cohesion for desert shrub species in the Lower Colorado riparian ecosystem and its potential for streambank stabilization. Ecological Engineering, **51**(1): 33-44.

ASTM D2487-11. 2011. Standard Practice for Classification of Soils for Engineering Purposes (Unified Soil Classification System), ASTM International, West Conshohocken, PA.

ASTM D4318-10e1. 2010. Standard Test Methods for Liquid Limit, Plastic Limit, and Plasticity Index of Soils, ASTM International, West Conshohocken, PA.

ASTM D6913-04(2009)e1. 2009. Standard Test Methods for Particle-Size Distribution (Gradation) of Soils Using Sieve Analysis, ASTM International, West Conshohocken, PA.

Barker, D. H. 1995. Vegetation and slopes: stabilisation, protection and ecology. *In* Proceedings of the international conference held at the University Museum, Oxford, 29-30 September 1994. Thomas Telford.

Bischetti, G. B., Chiaradia, E. A., Simonato, T., Speziali, B., Vitali, B., Vullo, P. and Zocco, A. 2005. Root strength and root area ratio of forest species in Lombardy, Northern Italy. Plant and soil, **278**(1-2): 11-22.

Bolton, M. D., Gui, M. W., and Phillips, R. 1993. Review of miniature soil probes for model tests. *In* Proceedings of 11th Southeast Asian Geotechnical Conference. Hong Kong, pp. 85-90.

Burylo, M., Rey, F., Roumet, C., Buisson, E., and Dutoit, T. 2009. Linking plant morphological traits to uprooting resistance in eroded marly lands (Southern Alps, France). Plant and Soil, **324**(1-2): 31–42

BS1377-2. 1990. Methods of test for soils for civil engineering purposes. General requirements and sample preparation. British Standards Institution.

Caicedo, B., and Tristancho, J. 2010. A virtual rain simulator for droplet transport in a centrifuge. *In* Proceedings of 7th international conference on Physical Modelling in Geotechnics (ICPMG 2010), Zurich, Switzerland. CRC Press.

Chiatante, D., Scippa, S. G., Di Iorio, A., and Sarnataro, M. 2003. The influence of steep slopes on root system development. Journal of Plant Growth Regulation, **21**(1)**:** 247–260.

De Baets, S., Poesen, J., Reubens, B., Wemans, K., De Baerdemaeker, J. and Muys, B. 2008. Root tensile strength and root distribution of typical Mediterranean plant species and their contribution to soil shear strength. Plant and Soil, **305**(1-2): 207-226.

Dell'Avanzi, E., Zornberg, J. G., and Cabral, A. R. 2004. Suction profiles and scale factors for unsaturated flow under increased gravitational field. Soils and foundations, **44**(3): 79-89.

Docker, B. B., and Hubble, T. C. T. 2008. Quantifying root-reinforcement of river bank soils by four Australian tree species. Geomorphology, **100**(1): 401–418.

Garg, A., Leung, A. K., and Ng, C. W. W. 2015. Comparisons of suction induced by evapotranspiration and transpiration of S. heptaphylla. Canadian Geotechnical Journal. 52(12): 2149 – 215.

Geotechnical Engineering Office (GEO). 2002. Investigation of some selected landslides in 2000. GEO report no. 131, Civil Engineering Department, Hong Kong.

Geo-Slope International Ltd. 2008. Stability Modeling with SLOPE/W, An Engineering Methodology, 4th Edition

Geo-Slope International Ltd. 2009. Seepage Modeling with SEEP/W, An Engineering Methodology, 4th Edition

Ghestem, M., Veylon, G., Bernard, A., Vanel, Q., and Stokes, A. 2014. Influence of plant root system morphology and architectural traits on soil shear resistance. Plant and Soil, **377**(1-2): 43-61

Greenwood, J. R., Norris, J. E., and Wint, J. 2004. Assessing the contribution of vegetation to slope stability. *In* Proceedings of ICE-Geotechnical Engineering. pp. 199-207.

Hau, B. C., and Corlett, R. T. 2003. Factors affecting the early survival and growth of native tree seedlings planted on a degraded hillside grassland in Hong Kong, China. Restoration Ecology, **11**(4): 483-488.

Ho, M. Y. 2007. Governing parameters for stress-dependent soil-water characteristics, conjunctive flow and slope stability. PhD Thesis, The Hong Kong University of Science and Technology

Hossain, M. A. and Yin, J. H. 2010. Shear strength and dilative characteristics of an unsaturated compacted completely decomposed granite soil. Canadian Geotechnical Journal, **47**(10):1112-1126.

Huang, B. 1999. Water relations and root activities of Buchloe dactyloides and Zoysia japonica in response to localized soil drying. Plant and Soil, **208**(2): 179-186.

Indraratna, B., and Redana, I. W. 2000. Numerical modeling of vertical drains with smear and well resistance installed in soft clay. Canadian Geotechnical Journal, **37**(1): 132-145.

Kamchoom, V., Leung, A. K., and Ng, C. W. W. 2014. Effects of root geometry and transpiration on pull-out resistance. Geotechnique Letters, **4**(1): 330-336. doi: 10.1680/geolett.14.00086.

Ladd, R. S. 1977. Specimen preparation and cyclic stability of sands. Journal of Geotechnical and Geoenvironmental Engineering, **6**(103): 535-547.

Lam, C. C., and Leung, Y. K. 1995. Extreme rainfall statistics and design rainstorm profiles at selected locations in Hong Kong. Hong Kong: Royal Observatory.

Leung, A. K., and Ng, C. W. W. 2013. Analysis of groundwater flow and plant evapotranspiration in a vegetated soil slope. Canadian Geotechnical Journal, **50**(12): 1204 – 1218.

Leung, A. K., Garg, A., and Ng, C. W. W. 2015. Effects of plant roots on soil-water retention and induced suction in vegetated soil. Engineering Geology. 193: 187 – 197.

Leung, A. K., and Ng, C. W. W. 2015. Field investigation of deformation mechanisms and stress mobilisation in a soil slope. Landslides, 13(2), 229 – 240.

Leung, T. Y. 2014. The use of native woody plants in slope upgrading in Hong Kong. PhD Thesis, The University of Hong Kong.

Li, P. W., and Lai, E. S. 2004. Short-range quantitative precipitation forecasting in Hong Kong. Journal of Hydrology, **288**(1): 189-209.

Lim, T. T., Rahardjo, H., Chang, M. F., and Fredlund, D. G. 1996. Effect of rainfall on matric suctions in a residual soil slope. Canadian Geotechnical Journal, **33**(4): 618-628.

Mickovski, S. B., and Ennos, A. R. 2003. Model and whole-plant studies on the anchorage capabilities of bulbs. Plant and soil, **255**(2): 641-652.

Miles, A.H., and Sheila, E. L. 1986. Plant Association and Management Guide. United States Department of Agriculture

Ng, C. W. W., and Leung, A. K. 2012. Measurements of drying and wetting permeability functions using a new stress-controllable soil column. Journal of Geotechnical and Geoenvironmental Engineering, ASCE, **138**(1): 58 – 65.

Ng, C. W. W., Kamchoom, V., and Leung, A. K. 2015. Centrifuge modelling of the effects of root geometry on transpiration-induced suction and stability of vegetated slopes. Landslides,**12**(5): 1-14.

Ng, C. W. W., Leung, A. K., and Woon, K. X. 2014a. Effect of soil density on grass-induced suction distributions in compacted soil subjected to rainfall. Canadian Geotechnical Journal, **51**(3): 311 – 321.

Ng, C. W. W., Leung, A. K., Kamchoom, V., and Garg, A. 2014b. A novel root system for simulating transpiration-induced soil suction in centrifuge. Geotechnical Testing Journal, **37**(5): 1–15.

Ng, C. W. W., Liu, H. W., and Feng, S. 2015. Analytical solutions for calculating pore water pressure in an infinite unsaturated slope with different root architectures. Canadian Geotechnical Journal, 52(12): 1981 – 1992.

Ng, C. W. W., Woon, K. X., Leung, A. K., and Chu, L. M. 2013. Experimental investigation of induced suction distributions in a grass-covered soil. Ecological Engineering, **52**(1): 219 – 223.

Powrie, W. 1986. The behaviour of diaphragm walls in clay. PhD Thesis, Cambridge University.

Ray, D., and Nicoll, B. C. 1998. The effect of soil water-table depth on root-plate development and stability of Sitka spruce. Forestry, **71**(2): 169-182.

Simon, A., and Collison, A. J. 2002. Quantifying the mechanical and hydrologic effects of riparian vegetation on streambank stability. Earth Surface Processes and Landforms, **27**(5): 527-546.

Sonnenberg, R., Bransby, M. F., Bengough, A. G., Hallett, P. D., and Davies, M. C. R. 2012. Centrifuge modelling of soil slopes containing model plant roots. Canadian Geotechnical Journal, **49**(1): 1 – 17.

Sonnenberg, R, Bransby, M. F., Hallett, P. D., Bengough, A. G., Mickovski, S. B., and Davies, M. C. R. 2010. Centrifuge modelling of soil slopes reinforced with vegetation. Canadian Geotechnical Journal, **47**(12): 1415 – 1430.

Stokes, A., and Mattheck, C. 1996. Variation of wood strength in tree roots. Journal of Experimental Botany, **47**(5): 693 – 699.

Taylor, R. N. 1995. Geotechnical Centrifuge Technology. Taylor and Francis.

van Genuchten, M. T. 1980. A closed-form equation for predicting the hydraulic conductivity of unsaturated soils. Soil Science Society of America Journal, **44**(5): 892-898.

Vanapalli, S. K., Fredlund, D. G., Pufahl, D. E., and Clifton, A. W. 1996. Model for the prediction of shear strength with respect to soil suction. Canadian Geotechnical Journal, **33**(3): 379-392.

Wang, C. L., Liu, J., Xing, H. W., Yao, X. J., Wang, L. H. & Niu, G. Q. 2010. Friction properties of interface between soil-roots and soil-soil of Artemisia sphaerocephala and Sabina

valgaris. *In* proceedings of 4th International Conference on Bioinformatics and Biomedical Engineering (iCBBE), Chengdu, pp. 1 – 5.

Wischmeier, W. H., and Smith, D. D. 1978. Predicting rainfall erosion losses: a guide to conservation planning. U.S. Department of Agriculture, Agriculture Handbook number 537, U.S. Government Printing Office, Washington (DC), pp. 58.

Yuan, F., and Z. Lu 2005. Analytical Solutions for Vertical Flow in Unsaturated, Rooted Soils with Variable Surface Fluxes. Vadose Zone Journal, **4**(4): 1210-1218.

Zhou, Z. B. 2008. Centrifuge and three-dimensional numerical modelling of steep CDG slopes reinforced with different sizes of nail heads. PhD Thesis, The Hong Kong University of Science and Technology

Zhu, H., and Zhang, L. M. 2015. Evaluating suction profile in a vegetated slope considering uncertainty in transpiration. Computers and Geotechnics. **63**(1): 112 – 120.

Table 1. Summary of the properties of CDG

Parameter		Value	Unit	Reference
Bulk unit weight (γ_t)		20	kN/m^3	Ho (2007)
Specific gravity (G_s)		2.59	-	
Maximum dry density		1890	kg/m^3	Standard Proctor compaction test (BS1377-2 1990)
Optimum moisture content		15.1	%	
Sand content ($\leq$ 4.760 mm)		56.8		Sieve Analysis (ASTM D6913-04(2009)e1)
Fine content ($\leq$ 0.074 mm)		43.2		
Plastic limit		22.7	%	Atterberg Limits test (ASTM D4318-10e1)
Liquid limit		32.8	%	
Plasticity index		10.1	%	
Effective cohesion (c')		0	kPa	Hossain and Yin (2010)
Critical-state friction angle (ϕ_{cr}')		37	degree	
Dilation angle (ψ)		5	degree	
Young's modulus (E)		35	MPa	Zhou (2008)
Poisson's ratio (ν)		0.26	-	
Saturated hydraulic conductivity (k_s)		$1x10^{-7}$	m/s	Falling head test (ASTM D5084-10)
Air-entry value (AEV)		1	kPa	Ho (2007)
Saturated water content (Θ_s)		See Fig. 1	%	SWRC measured by Ho (2007) and then fitted by van Genuchten (1980)
Residual water content (Θ_r)				
Fitting parameters for van Genuchten (1980)	α		kPa^{-1}	
	n		-	
	m			

Table 2. Summary of scaling factors and properties of model roots (after Ng et al. 2015)

Physical quantity	**Dimension***	**Scaling factor** (model/prototype)	**Model scale**	**Prototype scale**†
Geometry of root model				
Length	L	1/N	50 mm	750 mm
Outer diameter	L	1/N	6 mm	90 mm
Inner diameter	L	1/N	4 mm	60 mm
Cross-section area (A)	L^2	$1/N^2$	1.6×10^{-5} m^2	3.5×10^{-3} m^2
Second moment of inertia (I)	L^4	$1/N^4$	5.1×10^{-11} m^4	2.6×10^{-6} m^4
Material property of root model				
Tensile strength of root model (σ_t)	M/LT^2	1	3.1×10^4 kPa	3.1×10^4 kPa
Elastic modulus of root model (E)	M/LT^2	1	8.3×10^4 kPa	8.3×10^4 kPa
Axial rigidity (EA) of taproot	ML/T^2	$1/N^2$	1.3 kPa·m^2	2.9×10^2 kPa·m^2
Flexural rigidity (EI) of horizontal root branch	ML^3/T^2	$1/N^4$	4.2×10^{-6} kPa·m^4	2.2×10^{-1} kPa·m^4
Air-entry value of filter	M/LT^2	1	100 kPa	100 kPa
Hydraulic conductivity of filter	L/T_{diff}	N	2×10^{-6} m/s	1.3×10^{-7} m/s
Soil-atmosphere interface				
Rainfall intensity‡	L/T_{diff}	N	1050 mm/hr	70 mm/hr
Seepage				
Water flow rate	L^3/T_{diff}	1/N	Depend on measurements	
Hydraulic conductivity	L/T_{diff}	N		
Hydraulic gradient	--	1		
Suction (kPa) §	M/LT^2	1		

* Time for dynamic condition (T) is scaled by $1/N$, whereas time for diffusion (T_{diff}) is scaled by $1/N^2$

† Prototype scale at ***g***-level of 15 (i.e., $N = 15$)

‡ According to Talyor (1995)

§ According to Dell'Avanzi *et al.* (2004)

Table 3. Summary of centrifuge tests

Test ID	Slope angle	Root geometry	Root spacing	"Transpiration" phase		Rainfall phase	
				Vacuum pressure (kPa)	Transpiration duration (h)	Rainfall intensity (mm/h)	Rainfall duration (h)
T45	45	Tap	1.73 m x 1.73 m	95	120	70	8
T60	60						
H60		Heart					

Note: All dimensions in the table are expressed in prototype scale

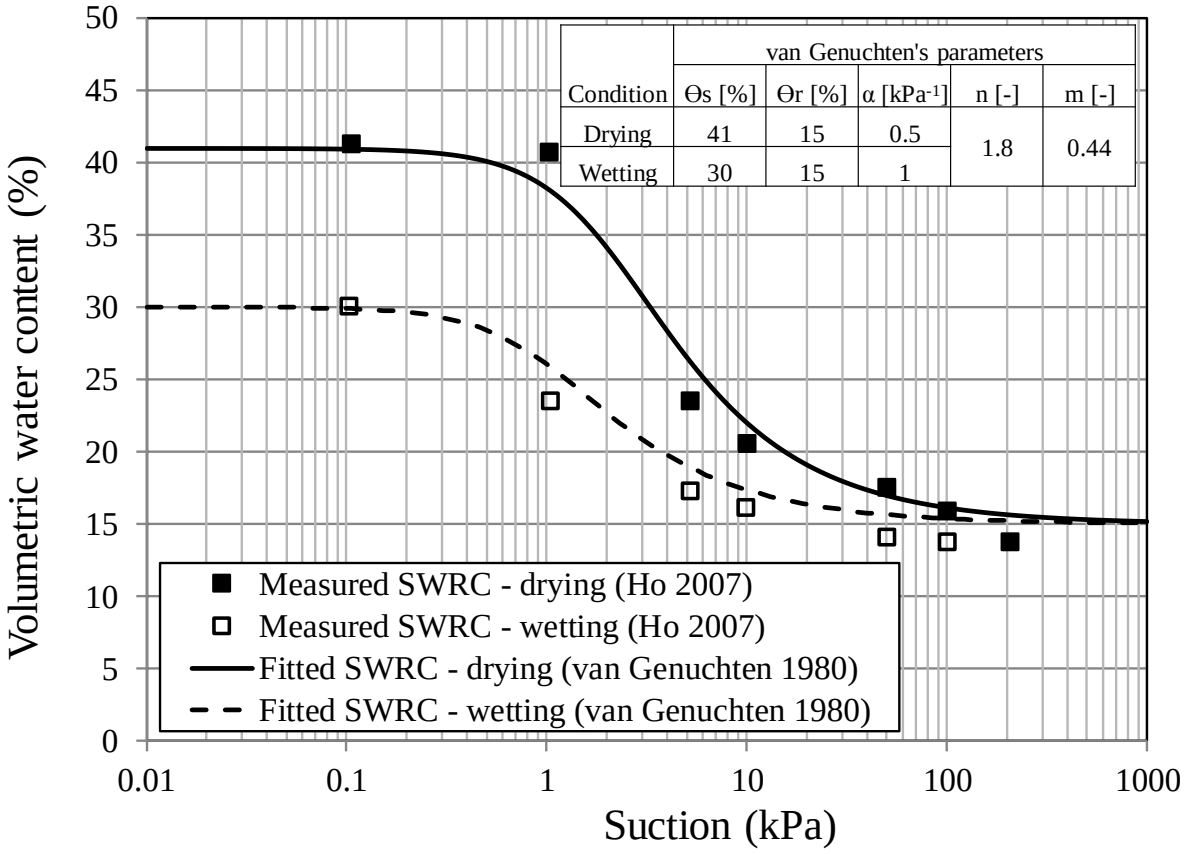

	van Genuchten's parameters				
Condition	Θs [%]	Θr [%]	α [kPa^{-1}]	n [-]	m [-]
Drying	41	15	0.5	1.8	0.44
Wetting	30	15	1		

Figure 1. Measured and fitted SWRCs of the CDG (Ng et al. 2015)

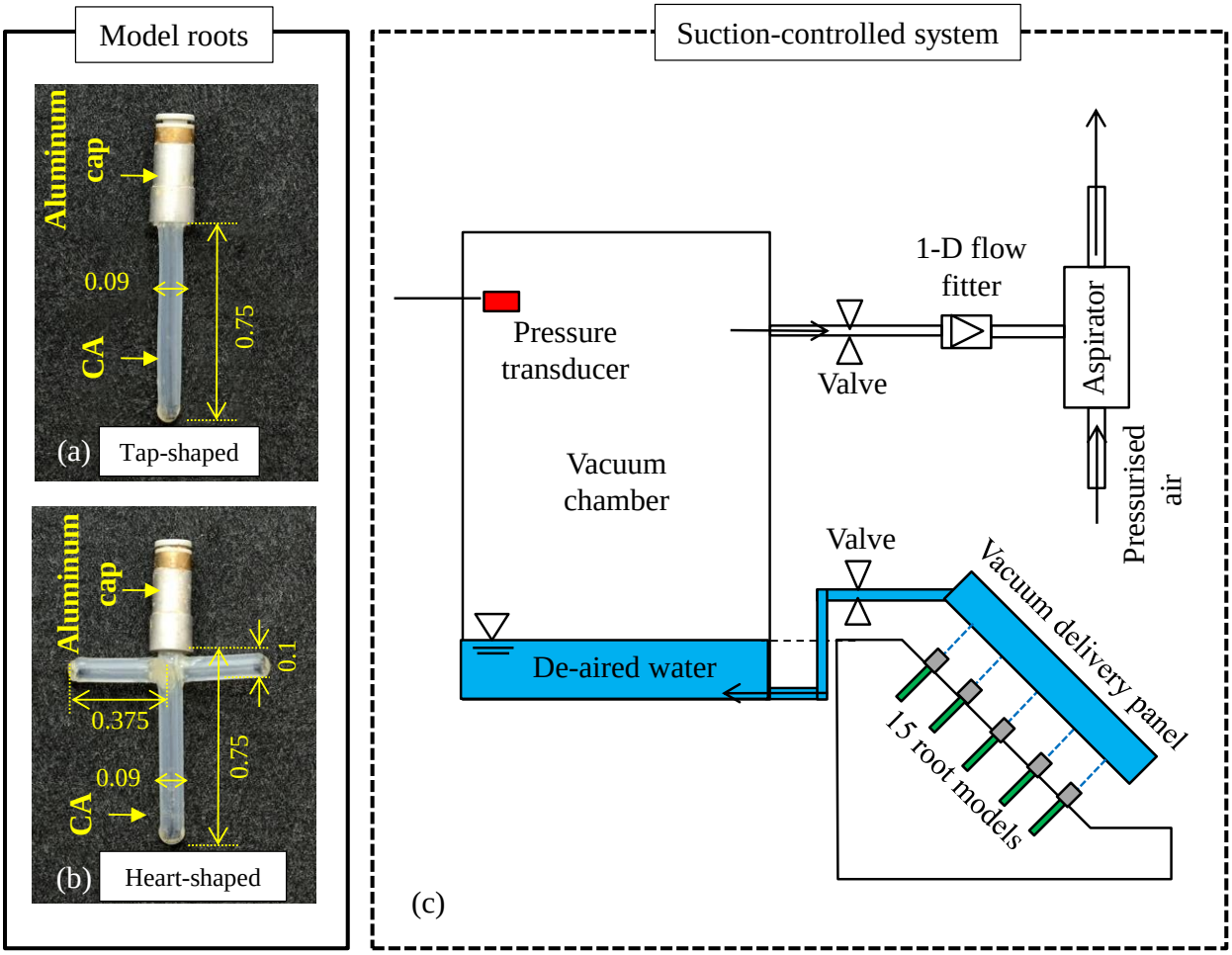

Figure 2. Overview of (a) tap-shaped and (b) heart-shaped model roots and (c) the suction-controlled system used to simulate the effects of transpiration in centrifuge (Ng et al. 2014b) (all dimensions are in meters and in prototype scale) (after Ng et al. 2015)

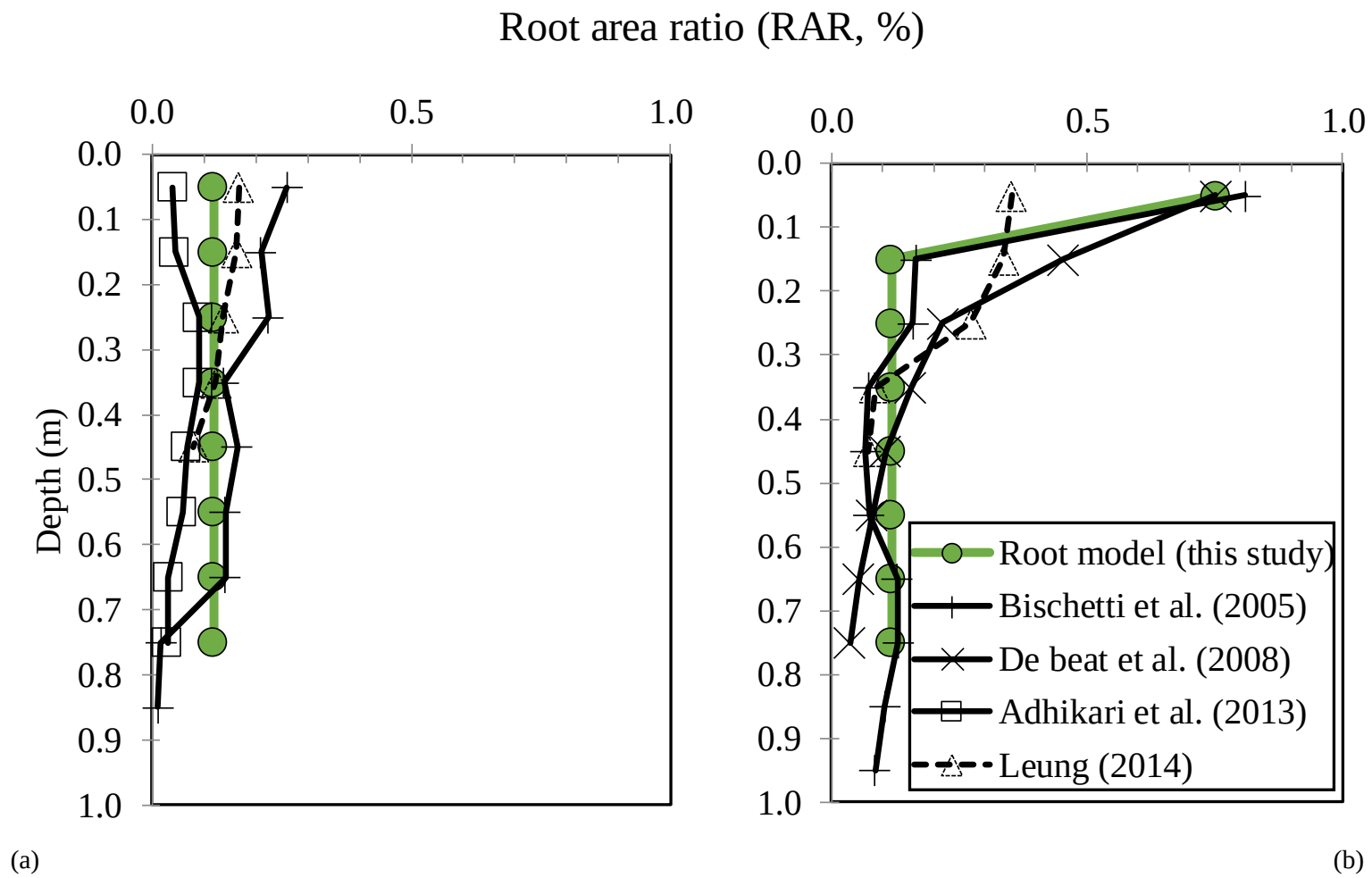

Figure 3. Comparisons of RAR profile of (a) tap-shaped and (b) heart-shaped roots with real roots found in the field

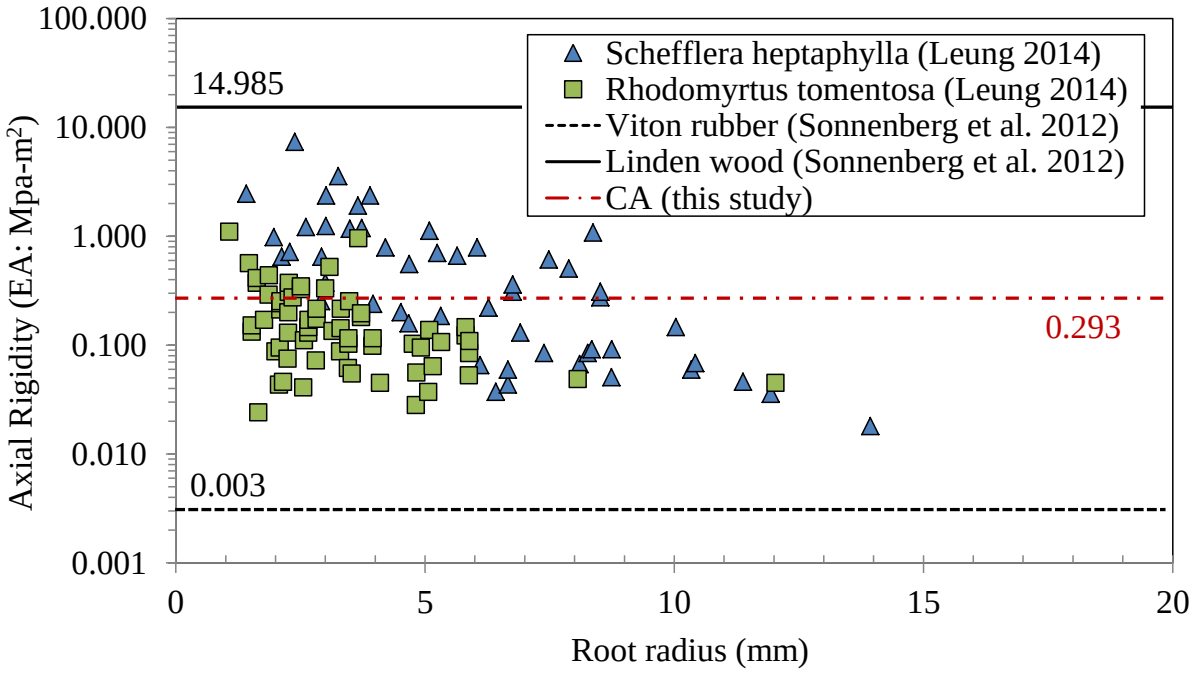

Figure 4. Comparisons of the axial rigidity of real roots and model roots (all units are in meters and in prototype scale)

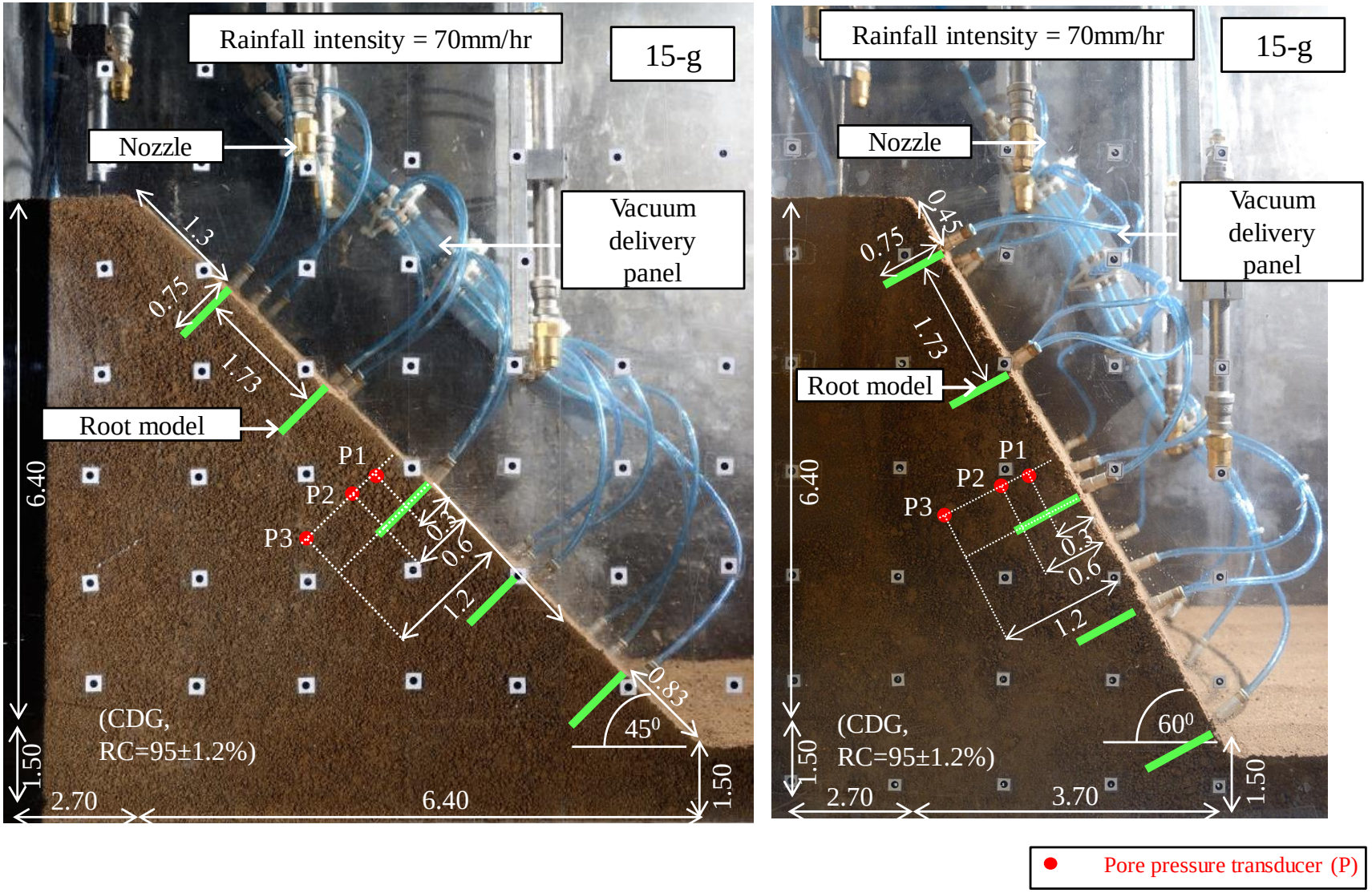

Figure 5. Centrifuge model setup for (a) Test T45 and (b) Test T60 (all dimensions are in meters and in prototype scale)

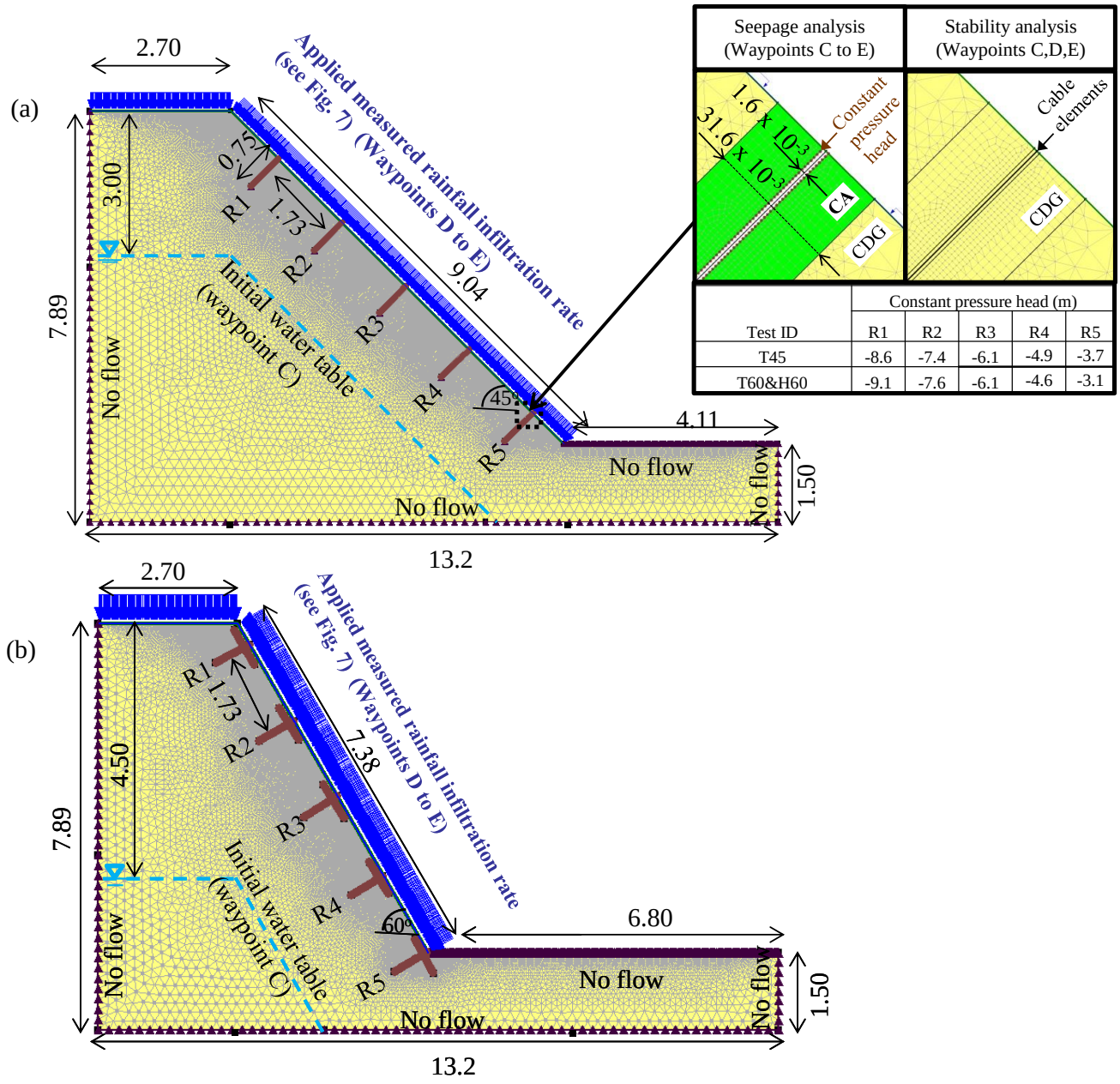

Figure 6. Typical finite element meshes and boundary conditions of transient seepage analyses for (a) Test T45 and (b) Test H60 (all dimensions are in meters and in prototype scale)

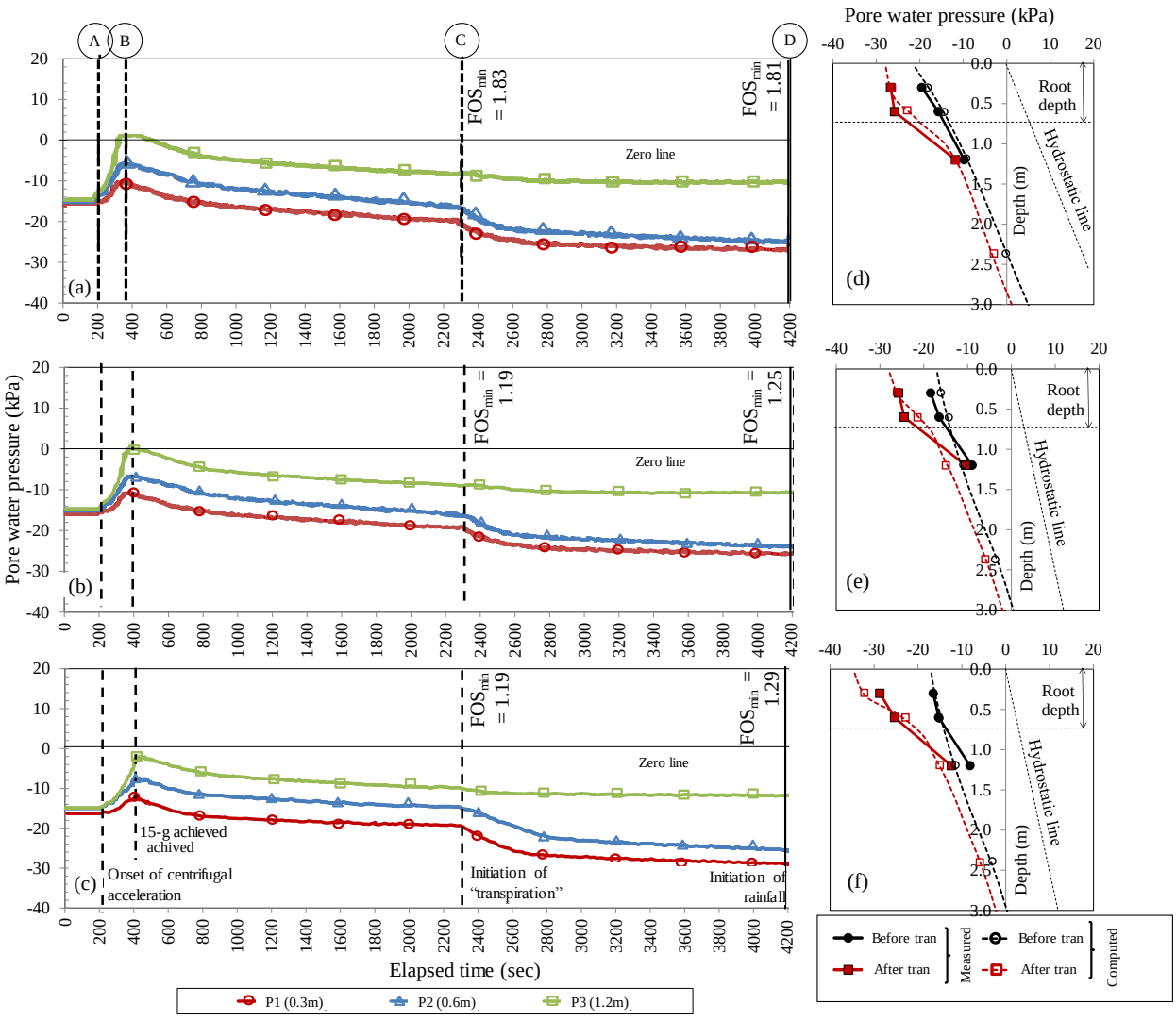

Note: "tran" in the legend denotes transpiration

Figure 7. Comparisons of the variations of suction with time for Tests (a) T45, (b) T60 and (c) H60 and the responses of PWP profiles for Tests (d) T45, (e) T60 and (f) H60 before rainfall

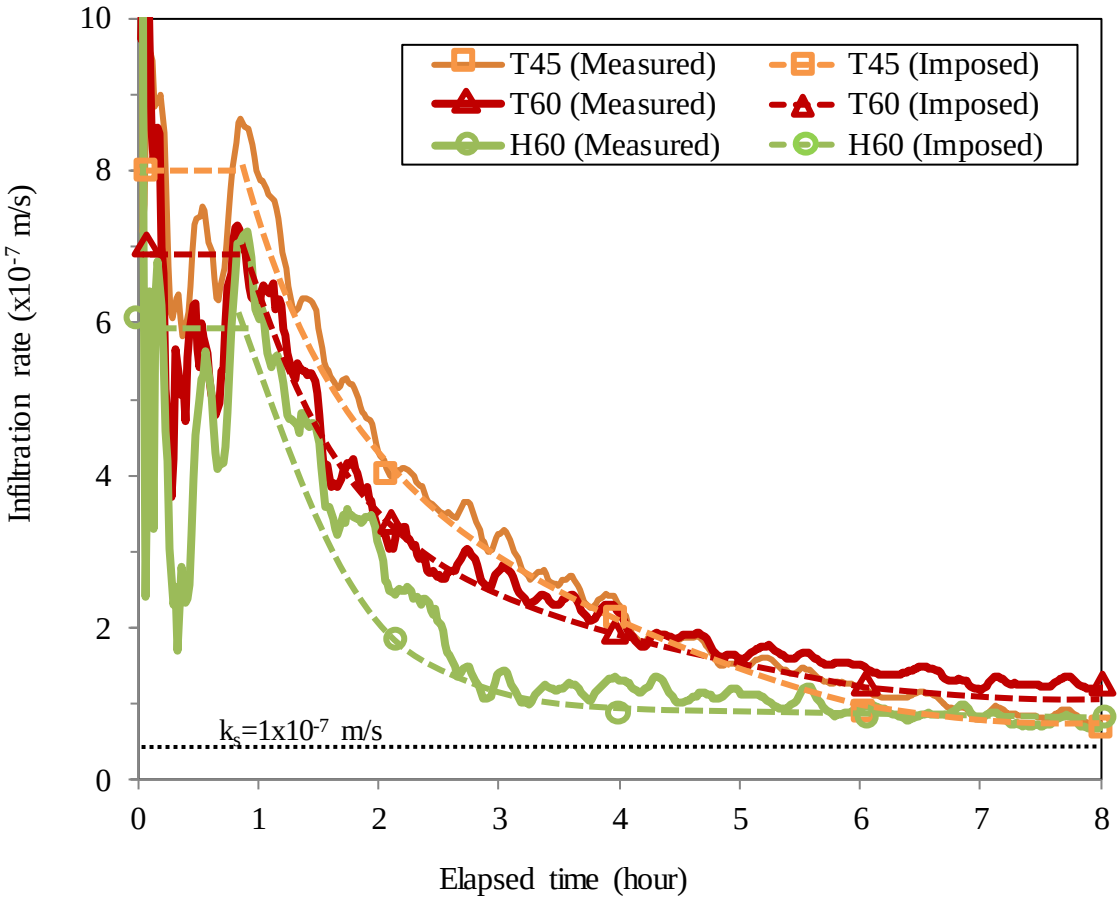

Figure 8. Measured and fitted infiltration rates for the three tests during the applied rainfall event

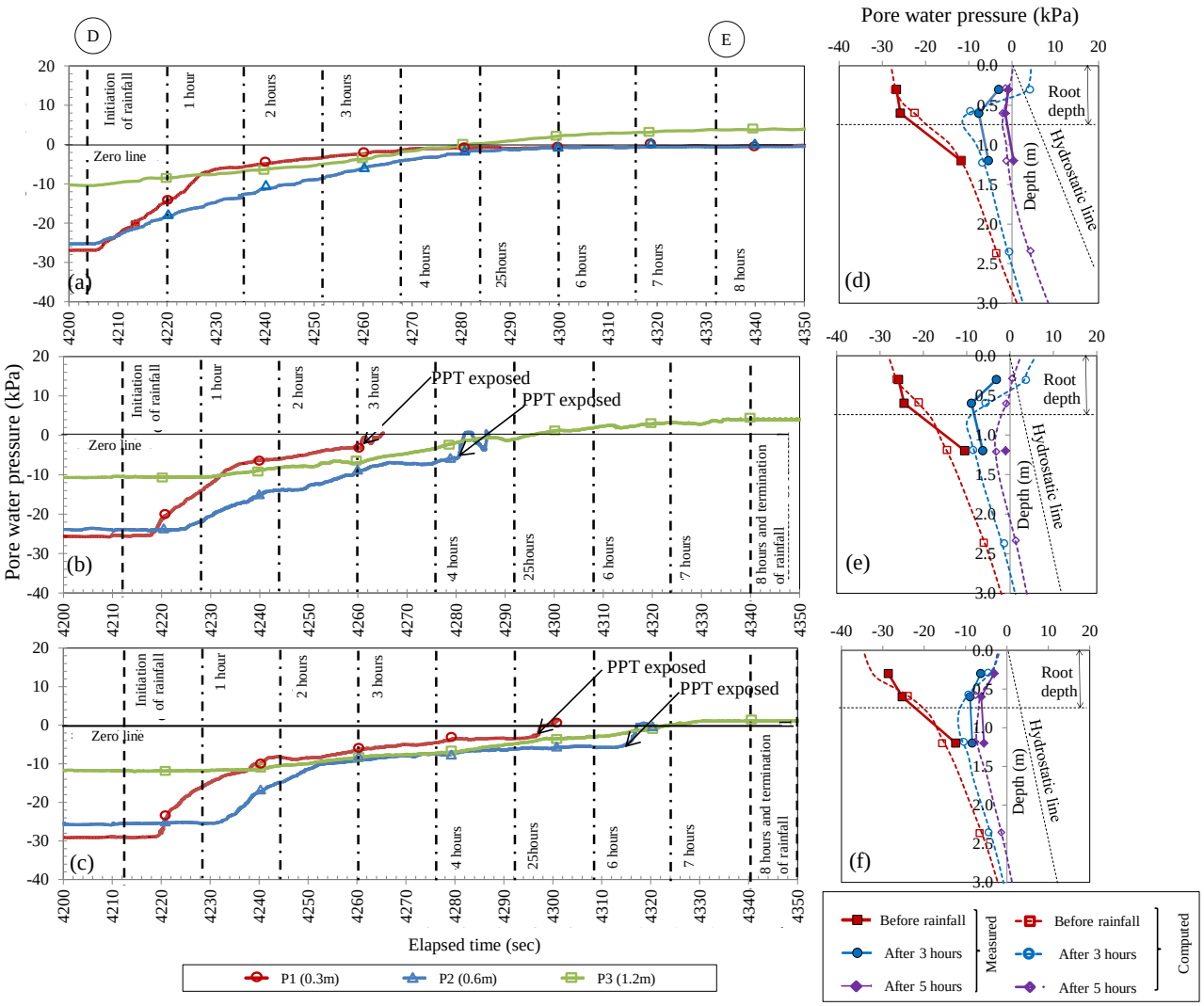

Figure 9. Comparisons of the variations of suction with time for Tests (a) T45, (b) T60 and (c) H60 and the responses of PWP profiles for Tests (d) T45, (e) T60 and (f) H60 during rainfall

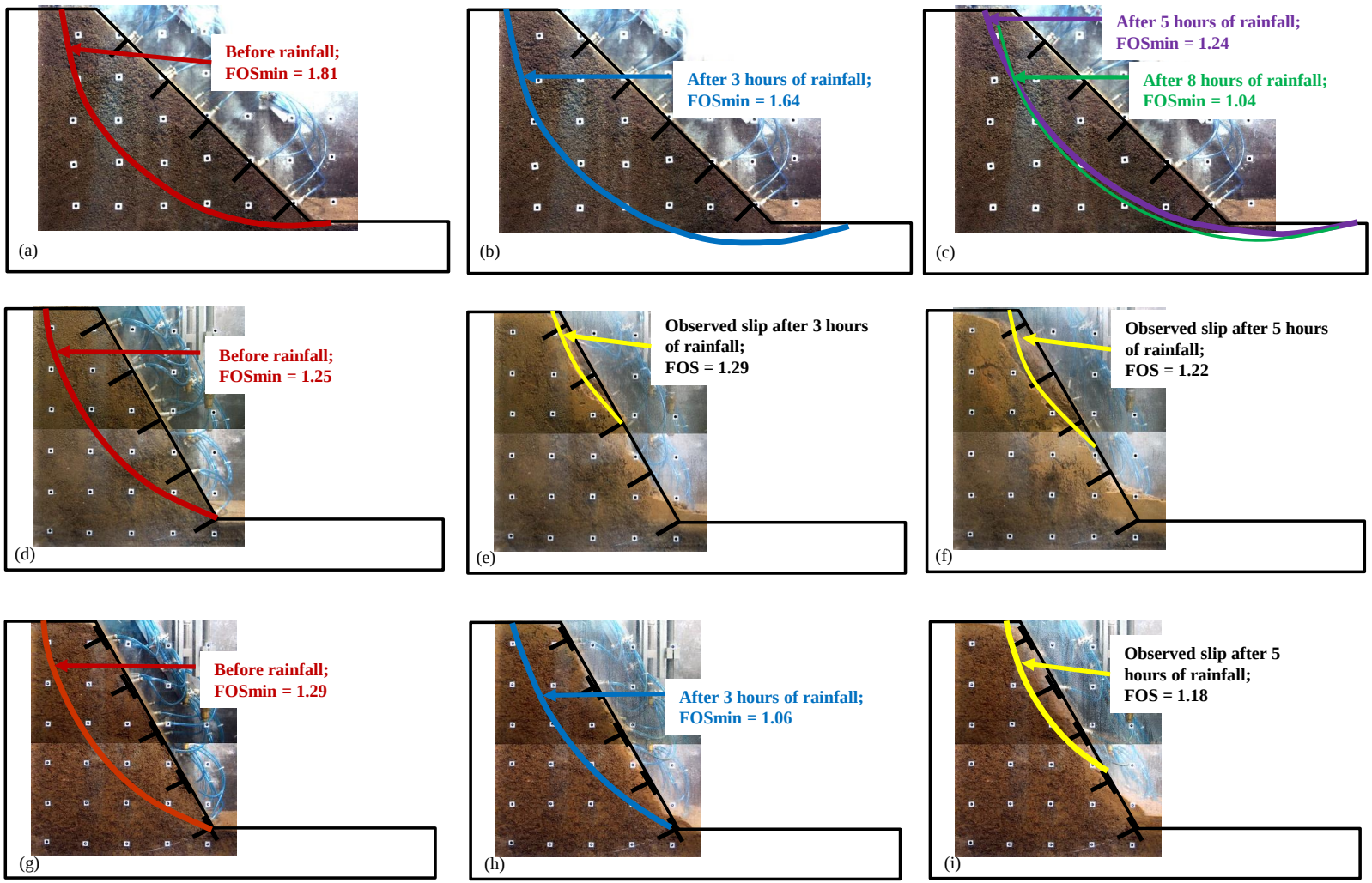

Figure 10. Images of model slopes and calculated FOS and FOS_{min} for Tests T45 ((a), (b), (c)), T60 ((d), (e), (f)) and H60 ((g), (h), (i)) before and after the rainfall event

1